



Liquid–liquid structure transition in metallic melt and its impact on solidification: A review

Yi-xuan HE^{1,2}, Jin-shan LI¹, Jun WANG¹, Eric BEAUGNON²

1. State Key Laboratory of Solidification Processing, Northwestern Polytechnical University, Xi'an 710072, China;
2. Université Grenoble Alpes, INSA Toulouse, Université Toulouse Paul Sabatier, EMFL, CNRS, LNCMI, 38000 Grenoble, France

Received 24 December 2019; accepted 21 July 2020

Abstract: Understanding the nature of liquid structures and properties has always been a hot field in condensed matter physics and metallic materials science. The liquid is not homogeneous and the local structures inside change discontinuously with temperature, pressure, etc. The liquid will experience liquid–liquid structure transition under a certain condition. Liquid–liquid structure transition widely exists in many metals and alloys and plays an important role in the final microstructure and the properties of the solid alloys. This work provides a comprehensive review on this unique structure transition in the metallic liquid together with the recent progress of its impact on the following microstructure and properties after solidification. These effects are discussed by integrating them into different experimental results and theoretical considerations. The application of liquid–liquid structure transition as a strategy to tailor the properties of metals and alloys is proven to be practical and efficient.

Key words: liquid–liquid structure transition; metals and alloys; thermal history; solidification

1 Introduction

Most metallic materials experienced one or several processes from liquid to solid before they were made into components. The process of liquid to solid has crucial influence on the mechanical and physical properties, and is related to lots of defects, especially metallurgical defects, which always leads to the failure of important components. As a result, investigation on the liquid metallic melts is of great importance and attracts a lot of attention.

In the past, the metallic melt was considered as homogenous and isotropic liquid according to the classical thermodynamics theory. However, as the

experimental and numerical methods were developed, recent research results show that the melt has short range order (SRO), medium range order (MRO), topological range order (TRO) etc, and the liquid state polymorphism is widely accepted [1–4]. Liquid–liquid structure transition (L–LST) is found to exist in almost all the materials, e.g., metallic melts [5–10], metalloid liquids [11,12], and molecular liquids [13,14]. It can be in either single component liquid like S [15], Si [16], P [11], C [17], Ca [18] and Te [19], or multi-component liquid, like $\text{Co}_{76}\text{Sn}_{24}$ [20], H_2O [21], SiC [22], Pd–Ni–P [23] and Fe–Si [24]. In this work, we mainly focus on the L–LST in metallic melts.

Foundation item: Project (51690164) supported by the National Natural Science Foundation of China; Project (2019-TS-04) supported by the State Key Laboratory of Solidification Processing, China

Corresponding author: Jin-shan LI, Tel: +86-29-88460294, E-mail: ljsh@nwpu.edu.cn;
Jun WANG, Tel: +86-29-88460568, E-mail: nwpuwj@nwpu.edu.cn

DOI: 10.1016/S1003-6326(20)65380-8

2 Basic concepts of liquid–liquid structure transition

There is no ideal model to describe the liquid structure because of its uncertainty and instability. Different from the crystal structure, liquid structure is non-symmetric and long-range disordered. Experiments and numerical simulation results show that there are nomadic atom clusters surrounded by free atoms in the liquid and the size of these clusters changes with temperature. Except thermal expansion, there are growing experimental and theoretical supports for the existence of thermal contraction of atom clusters in the heating process [25–28].

2.1 Classification of L–LST

A single-component liquid may have more than two kinds of isotropic liquid states and the transition among these different states is called L–LST [29]. In general, according to the condition in which it occurs, L–LST can be classified as pressure induced L–LST, temperature induced L–LST and other external physical field induced L–LST. Pressure induced L–LST mostly occurs in molecular liquid such as C [17] and P [11]. Since the influence of pressure on metallic melt is less obvious than that on the molecular liquid, the L–LST in metallic melt is mostly induced by temperature, some other external physical field or the effect of both.

Another classification of L–LST is based on the reversibility of the transition process, namely reversible L–LST and irreversible L–LST. Figure 1(a) shows the temperature dependence of nuclear magnetic resonance (NMR) observable in metallic glass forming liquid $\text{La}_{50}\text{Al}_{35}\text{Ni}_{15}$ [30]. In situ high-temperature ^{27}Al NMR experiments were carried out above the liquidus temperature (970 K). The NMR spectrum at temperature above liquidus temperature presents a single narrow peak of Lorentzian shape. The peak position of spectrum representing the Knight shift (K_s) is sensitive to the changes of structures. NMR spectra were taken every 1 K interval during the cooling and reheating process. The corresponding K_s versus T is shown in Fig. 1(a). The cooling curve of K_s varies linearly with T from 1143 down to 1013 K with a slope of $0.22 \times 10^{-6} \text{ K}^{-1}$, followed by a sharp drop at 1013 K,

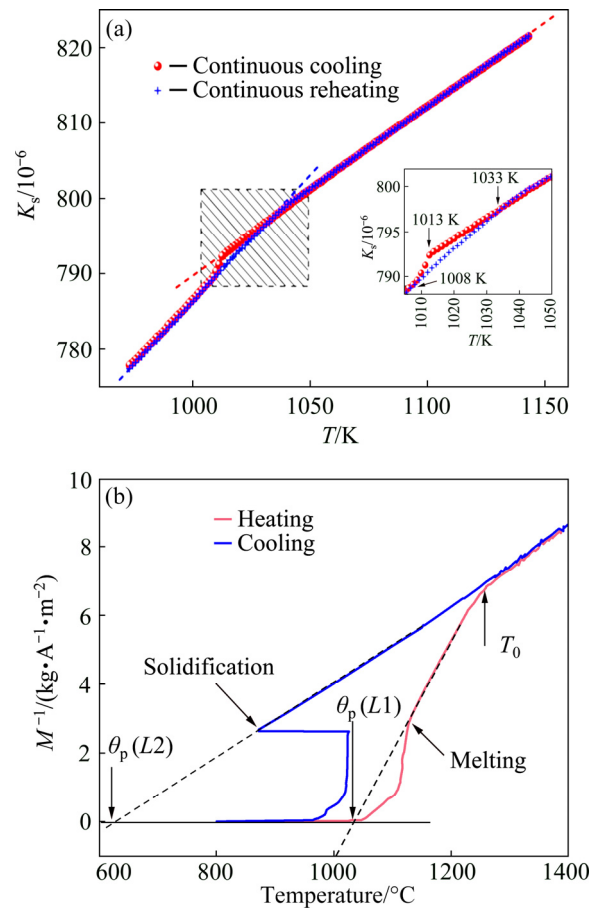


Fig. 1 Temperature dependence of Knight shift (K_s) during continuous cooling and reheating in temperature interval of 973–1143 K [30] (a) and M^{-1} – T curve of $\text{Co}_{76}\text{Sn}_{24}$ alloy measured in 1 T magnetic field [20] (b)

and then continues with a linear T -dependence down to 973 K with a slope of $0.33 \times 10^{-6} \text{ K}^{-1}$. The continuous reheating curve of K_s reproduces the values of the cooling curve except a hysteresis in the temperature range of 1008–1033 K, which is due to the undercooling effect. The kink at 1033 K identified by the slope change suggests a temperature-induced L–LST and the reproduction of K_s in the subsequent reheating process indicates that this transition is reversible. The change of inverse magnetization (M^{-1}) as a function of temperature of $\text{Co}_{76}\text{Sn}_{24}$ alloy is shown in Fig. 1(b) [20]. During heating, a net change in slope is observed at T_0 (1255 °C), indicating the structure transition in the liquid. However, during cooling, M^{-1} – T curve overlaps with the heating curve above T_0 but remains continuous with the same slope below T_0 and does not show the change in slope during heating, which suggests that the liquid structure change is irreversible.

However, the mechanism of reversible and irreversible L–LST is not clear so far, and it is believed to be related to the species of the SROs and the properties of elements. For example, LI et al [31] consider that there may be two types of SROs in the initial Sn–3.5Ag–3.5Bi melt: one is the irreversible metastable SROs (e.g., Bi–Bi and 65Sn–35Ag), and the other is the reversible tetrahedral SROs with covalent characteristics (e.g., Sn–Sn). Metastable SROs can exist for a long time at low temperature and will be broken to generate new atomic clusters or dissolve to form smaller SROs once the temperature surpasses the critical turning point to make the melts more disordered. However, the newly-generated SROs cannot be recovered during the subsequent cooling process, which leads to irreversible L–LST. In contrast, the reversible SROs dissipate during heating and can be rebuilt during cooling, which leads to reversible L–LST. A more in-depth analysis of the structure and stability of local favored structures in different temperature ranges will be required to further study the mechanism of the reversible and irreversible L–LST.

Furthermore, the existence of L–LST can be evidenced either in an overheated liquid or in an undercooled liquid. For instance, YU et al [32] studied the resistivity versus temperature (ρ – T) behaviors of liquid $\text{Bi}_2\text{Te}_{2.7}\text{Se}_{0.3}$ alloy and a clear hump is observed during the heating process, indicating that a temperature-induced L–LST takes place in the overheated liquid (Fig. 2(a)). Time-resolved synchrotron measurements were conducted to capture the structure evolution in the supercooled $\text{Zr}_{57}\text{Nb}_5\text{Al}_{10}\text{Cu}_{15.4}\text{Ni}_{12.6}$ liquid and the results show a crossover in the liquid structure at about 115 K below the melting temperature, indicating that a temperature-induced L–LST takes place in the undercooled liquid (Fig. 2(b)) [33].

2.2 Mechanisms and thermodynamics of L–LST in metallic melt

The mechanism of L–LST refers to the content and the behavior of atomic clusters, namely SROs and MROs, which is related to the properties of elements. TANAKA [29] held the view that liquid is not homogeneous and locally favored structures exist in liquid. The nearest-neighbor coordination difference leaves space for local structural variation of chemical and topological order [34]. Therefore,

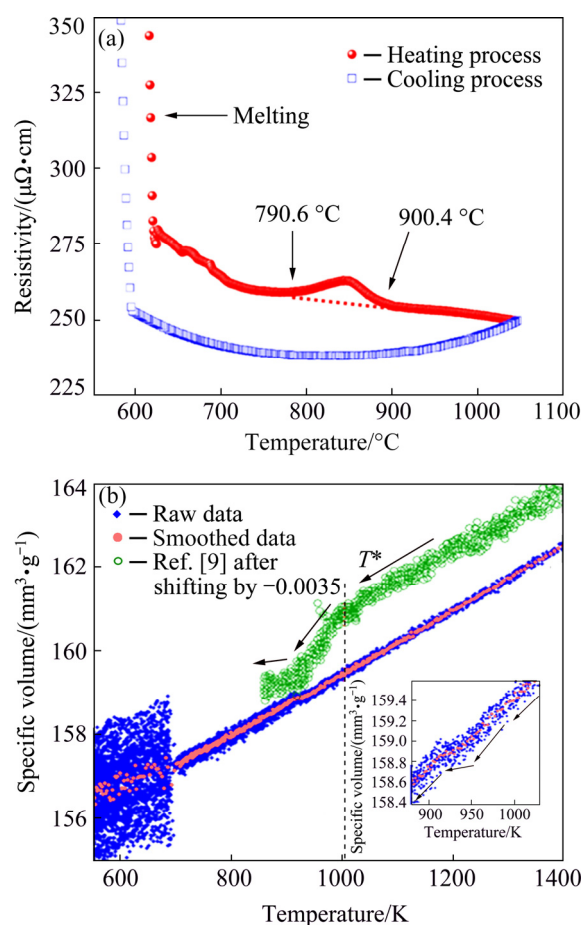


Fig. 2 Liquid–liquid structure transition in $\text{Bi}_2\text{Te}_{2.7}\text{Se}_{0.3}$ melt in overheated state [32] (a) and in $\text{Zr}_{57}\text{Nb}_5\text{Al}_{10}\text{Cu}_{15.4}\text{Ni}_{12.6}$ liquid in undercooled state [33] (b)

the SROs (even MROs) of liquid might vary with temperature, resulting in the change of thermodynamic properties. There are growing experimental and theoretical supports for the existence of L–LSTs in metallic melts and plausible three-dimensional structural models can be reconstructed via simulation methods such as reverse Monte Carlo [35], ab initio molecular dynamics (AIMD) [36,37], and cluster alignment method [34]. Figure 3 shows the three-dimensional representation of average SRO of liquid Ga at the selected four temperatures using the recently-developed cluster alignment method, which describes the local atomic packing and has been applied to directly visualizing the average local SRO and MRO in the liquid [34]. At 1600 K, the aligned clusters exhibit weak SRO, indicating a highly disordered structure. The local SRO enhances in the cooling process and the crystalline orthorhombic-like local atomic packing is detected at 600 K. Combined with high-temperature and

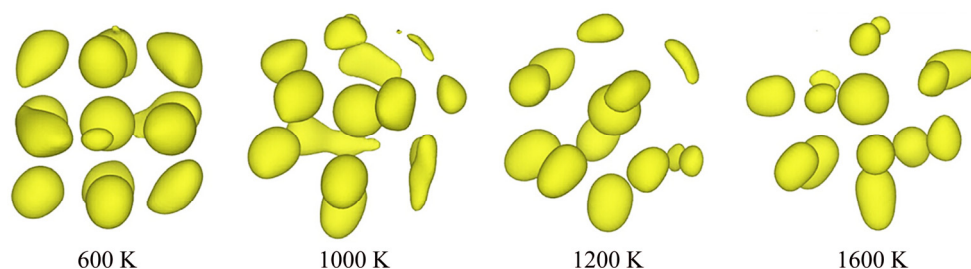


Fig. 3 Atomistic morphology evolution in liquid Ga obtained using cluster alignment method [34]

high-energy XRD measurements and AIMD simulations, an intriguing liquid structure change between two different Ga liquid regimes is discovered; i.e., the high-coordinated orthorhombic-like atomic packing at low temperature in liquid is broken up during heating and transforms into low-coordinated disordered polyhedrons at high temperature region.

TANAKA [29] proposed that an L–LST can be predicated on two order parameters, i.e., density and bond ordering. The density ordering parameter maximizes the density (or packing) to lower the attractive interaction energy, which ultimately leads to long-range ordering or crystallization. The bond ordering parameter describes the packing of locally favored structures, which captures both SRO and MRO. The liquid is in an excited state at high temperatures and transforms into an energetically more favorable state with higher density as the temperature decreases. IWASHITA et al [38] studied the liquid state of several metallic systems through classical and AIMD simulations. The results suggested that elementary excitations in high-temperature metallic liquids are local configurational changes in the atomic connectivity network. The L–LST is attributed to the competition between the configurational excitations and phonons. However, a rigorous experimental observation of L–LST is still deficient because of the harsh conditions in experiments, including (1) high temperature (and often high pressure), and/or (2) deep in the undercooling regime where crystallization is prone to occur. As a result, the mechanism of L–LST remains still inconclusive to date.

ZU [39] assumed that L–LST is a transition from an inhomogeneous liquid state to a more uniform liquid state. There are both chemical and topological SROs in the liquid alloys with negative

excess enthalpy. These minor domains as the fluctuation of energy dissipate and engender with time and space, but they do not vanish with their statistical equilibrium structures, sizes and constituents. However, as long as the temperature surpasses the critical turning point, the inter-atomic bonds in the original domains are broken, the old domains are reduced and at the same time, new domains form with a relatively more uniform liquid structure state. Therefore, L–LST is thought to be entropy-driven, which have been verified by the thermal effect on the DSC and DTA curves in many liquid systems [40–42].

3 Methods to characterize L–LST

So far, a lot of efforts have been made to study the liquid metal and many experimental and numerical evidences have been accumulated for the existence of the L–LST in metallic liquids. The experimental methods on L–LST research are mainly focused on detecting the liquid structure and they can be sorted into direct measurement and indirect measurement roughly. The direct methods could be classified into diffraction methods and absorption methods. The main mechanism of diffraction method on L–LST research is the diffraction of neutron, electron or X-ray. The absorption methods are based on the radiation scattering. Indirect methods measure the physical parameters that have close relationship with the liquid structure.

3.1 Experimental methods

3.1.1 Direct methods to study L–LST

Direct methods are effective and accurate ways to analyze liquid structure, which offer the average and one-dimensional structural information of the liquid state directly. The direct methods can be

classified into diffraction methods and absorption methods according to the mechanism utilized. The structure of the liquid state can be exhibited accurately by the parameters obtained by diffraction methods or absorption methods such as radial distribution function (RDF) $g(r)$, mean nearest neighbor distance r_1 and coordination number N_1 .

Common diffraction methods include X-ray diffraction, electron diffraction and neutron diffraction which are based on the diffraction of X-ray, electron and neutron, respectively [43]. Neutron scattering lengths mainly depend on nuclear mass, and X-ray scattering lengths depend on the number of electrons. These two techniques provide complementary information for a polyatomic liquid or glass [44]. Besides, neutron is electro-neutral but it has magnet moments, leading to deep penetration and magnetic diffraction when it is utilized on magnetic materials. Up to now, to investigate the atomic scale structure of metallic liquid, the most frequently used X-ray diffraction methods are energy dispersive X-ray diffraction (EDXD) [45,46], high energy synchrotron X-ray diffraction (HESXRD) [5,34,47], small-angle X-ray scattering (SAXS) [48], and wide-angle X-ray scattering (WAXS) [48].

Compared with the usual diffraction methods, X-ray absorption fine structure (XAFS) [49], an absorption method, has the advantage of providing information in respect of the local atomic arrangement around a specific atomic species. On the contrary, a diffraction experiment gives the information of atomic arrangements around a reference atom which represents an average of all atomic species present in the specimen [50]. Furthermore, X-ray absorption phenomenon depends on the effect of SRO, so XAFS is always an effective method no matter the atoms in the system are periodic or not.

High temperature nuclear magnetic resonance (NMR) [30] can also be used to detect structure changes in metallic melt; however, there is just quite few result about metallic melts up to now due to its difficulty.

3.1.2 Indirect methods to study L–LST

Indirect methods are widely applied due to the limit and the high cost of direct methods. Physical parameters sensitive to the liquid structure are selected. Physical parameters such as density [51], heat capacity [52], internal friction [53], magnetic

susceptibility [54], resistivity [55], viscosity [56–58], and specific volume [59], can be chosen to detect the changes of the liquid structure, and the structure and the working principle of the instruments are relatively simple and effective.

Compared to other physical parameters and the derived methods, the magnetic susceptibility and its corresponding method [60] have obvious advantages. On one hand, by in-situ measuring the temperature and magnetization, the melting behavior, the solidification process and other possible transformations (e.g., the eutectoid transformation: $\text{Co}_3\text{B} \rightarrow \text{Co}_2\text{B} + \alpha\text{-Co}$) can be observed, as shown in Fig. 4(a). Even the small difference of the soluble boron concentration between the primary $\alpha\text{-Co}$ phase and the $\alpha\text{-Co}$ phase forming subsequently during the eutectic transformation can be detected. As shown in Fig. 4(a), during the heating process, two magnetization drops are observed before melting, which are thought to be attributed to the variance of solid solubility of boron in the $\alpha\text{-Co}$ phase. Because of the non-equilibrium solidification process, the soluble boron concentration in the primary or subsequently $\alpha\text{-Co}$ phase forming during eutectic transformation could be different and the resultant Curie temperatures are different. On the other hand, with the help of glass fluxing technique, the magnetization of the liquid alloy can be in-situ measured in a very wide temperature range from hundreds of degrees above the melting point (overheated state) to hundreds of degrees below the melting point (supercooled state). As a consequence, this method can be used to study the possible L–LST either in the overheated state or in the supercooled state.

Above the melting point, the sample turns to be a fully paramagnetic liquid. Consequently, its susceptibility obeys the Curie–Weiss law. The relationship between the magnetization and temperature is given as

$$\frac{1}{M} = \frac{T - \theta_p}{HC} \quad (1)$$

where H , C and θ_p are the applied field, the material-specific Curie constant and the paramagnetic Curie temperature, respectively. Accordingly, θ_p can be determined from the M^{-1} versus T curve by extrapolating the curve to the point where $1/M$ equals zero. Figure 4(b) shows the

plot of M^{-1} versus T . During heating, a distinct crossover dividing the curve into two linear segments with different slopes is observed at T_0 (~ 1553 K). The crossover observed can be interpreted as being related to the magnetism of Co ions in the melt and the change in their coupling. Hence, the crossover at T_0 during heating demonstrably indicates a temperature-induced L–LST in the overheated $\text{Co}_{81.5}\text{B}_{18.5}$ alloy. Similar non-Curie–Weiss behavior but different values of characteristic parameters were observed in the Co–B binary alloy system [61]. The variation tendencies of these parameters with increasing the content of Co are shown in Fig. 5. The locations of the critical point of L–LST (T_0) and paramagnetic Curie temperatures (θ_p) for Liquids 1 and 2 shift to higher temperature with increasing the content of Co, which is thought to be due to the type, amount and size of the locally favored structures, e.g., the Co-rich domains and Co_3B -like configuration of Co–B pairs vary with the composition.

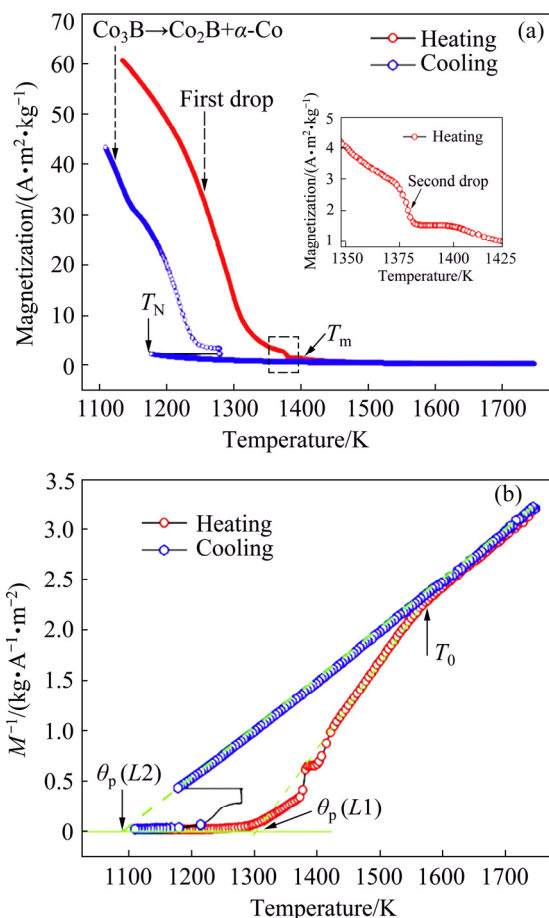


Fig. 4 Temperature dependence of magnetization for $\text{Co}_{81.5}\text{B}_{18.5}$ alloy measured in field of 1.56 T with field gradient of 23.235 T/m (a) and inverse magnetization (M^{-1}) plotted against temperature (b) [54]

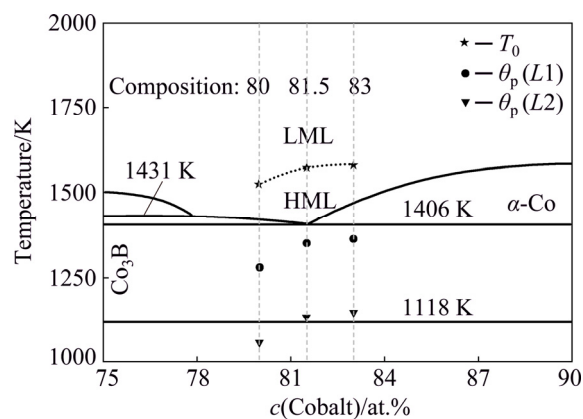


Fig. 5 Co-rich region of Co–B phase diagram [62] (Symbols are points for determining characteristic parameters [61])

3.2 Simulation methods

Recently, using computer calculation to investigate the structure of liquids, especially under extreme condition such as high pressure, high temperature and deep supercooling, which is known as ‘No man’s land’ [63], has attracted deep interesting around the world. So far, many methods such as Monte Carlo simulations [63], reverse Monte Carlo analysis [35], phase field calculations [64], free energy methods [65], molecular dynamics simulations [66–75], ab initio molecular-dynamics simulations [18,24,69,76], first-principles calculations [77] and combination of both methods, i.e., first-principles molecular dynamics [78], were adopted to study L–LST and had already made certain progress. For example, ZHAO et al [79] studied the structural evolution in Cu–Zr alloys by molecular dynamics (MD) simulations. The analysis results are shown in Figs. 6(a–c). Figure 6(a) shows the temperature evolution of the average of R_c (cutoff distance determines the neighborhood between atoms), which reflects the global characteristic of MRO structures in the system. Three different liquid states, high temperature zone (HTZ), abnormal zone (AZ) and low temperature zone (LTZ), can be identified with the slope changes at 1260 and 1000 K. Figure 6(b) shows the temperature evolution of two representative structural units in amorphous alloys, i.e., Z12 and A13. The Z12, one of the most important building blocks in the amorphous CuZr alloys, acceleratedly increases in AZ and LTZ. Figure 6(c) shows the average sharing index of icosahedrons as a function of temperature,

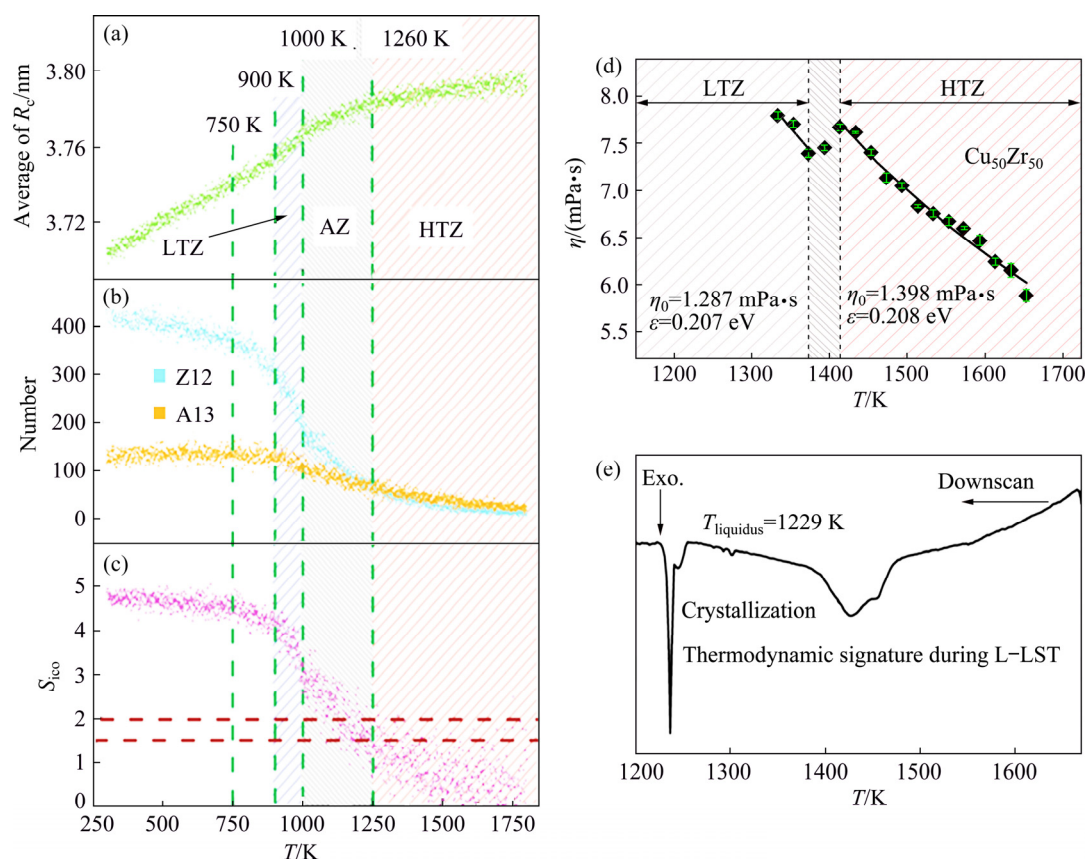


Fig. 6 Structural evidence of L–LST in $\text{Cu}_{50}\text{Zr}_{50}$ alloy obtained from MD simulation [79] (a–c) and experimental characterization [56,79] (d, e): (a) Average of cutoff distance R_c , confining neighborhood space around certain center atom; (b) Number of Z12 and A13, two representative structural units of amorphous alloys; (c) Average sharing index of icosahedrons, S_{ico} , average number of shared atoms between icosahedrons; (d) Equilibrium viscosity data versus T during cooling; (e) DSC down-scan curve cooled at 10 K/min

indicating that the interconnection enhancement of icosahedrons accelerates in AZ and LTZ. All these simulation results demonstrate that the existence of L–LST during solidification of CuZr alloys, which is consistent with the experimental results in Figs. 6(d, e). Figure 6(d) shows the temperature dependence of the viscosity of CuZr alloy upon cooling with a three-stage tendency feature similar to the MD simulation, i.e., HTZ, AZ and LTZ. A viscosity drop corresponding to the L–LST can be observed in the AZ. In the same temperature range, an exothermic peak is detected, as shown in Fig. 6(e).

4 Effects of L–LST on solidification

There has been a notable trend in engineering practices that the properties and solidified microstructures of many alloys are dependent on thermal history of their parent liquids [32,80,81].

The alteration of the solidification microstructure in different thermal histories is thought to be ascribed to different liquid states. Therefore, controlling the liquid states, based on the L–LSTs, has been confirmed to be effective in regulating the subsequent solidification processes, microstructures and properties.

4.1 Nucleation

Nucleation is an activated process in which the system has to overcome a free energy barrier in order for a first-order phase transition between the metastable and the stable phases to take place [82]. The ability to control nucleation is the key of the development of novel microstructures for advanced materials [83]. The ordering structure can be the precursor of nuclei in the metallic liquids, and thus any structure transition inside the metallic melt can make the nucleation process different.

According to the classical nucleation theory,

nucleation can be classified into homogeneous and heterogeneous nucleation. Homogeneous nucleation in pure metals occurs with an undercooling around 0.2 time liquidus temperature, and heterogeneous nucleation depends on the kind of substrates present in the melt. By using appropriate techniques, e.g., levitation and melt fluxing, heterogeneous nucleation can be restrained, which makes it possible to study the effect of L–LST on the nucleation.

YU et al [32] studied the solidification behavior of $\text{Bi}_2\text{Te}_{2.7}\text{Se}_{0.3}$ alloy in different liquid states, based on the temperature-induced L–LST detected by resistivity measurements during the heating process. As shown in Fig. 7, the sample that experienced L–LST shows that the nucleation and growth undercooling degrees are significantly enlarged and the solidification time is shortened. The atomic bonds of crystals are only partly broken on melting. The SROs similar to the corresponding solid crystal still remain in overheated melt within a certain temperature range. These SROs as the intrinsic growth nuclei can lead to the variation of

undercooling [84]. When an alloy is melted below the L–LST temperature, the SROs can easily become the core of nucleation, which promote the nucleation during cooling. At a temperature higher than that of the L–LST, these SROs break or dissolve to generate new atomic clusters. The SROs then become more uniform and disordered, changing the melt state. These changes impact solidification by inducing a much smaller critical nucleation radius, R^* . In addition, since the solid-like clusters are destroyed during the L–LST process, the structural mismatch at the solid–liquid interface is exaggerated. Therefore, the solid–liquid interface energy (σ_{ls}) should be higher for the samples experiencing L–LST. According to the classical nucleation theory, the undercooling degree for nucleation, ΔT , can be expressed as

$$\Delta T = \frac{2\sigma_{\text{ls}}V_m T_m}{\Delta H_m R^*} \quad (2)$$

where V_m is the molar volume of nucleation crystal, T_m is the melting point, and ΔH_m is the latent heat of fusion. Therefore, the undercooling will rise with σ_{ls} increasing and R^* decreasing.

WANG et al [7] evidenced an L–LST in the overheated $\text{Co}_{83}\text{B}_{17}$ alloy, and they found that the L–LST has strong influence on the nucleation temperature of undercooled melt. As shown in Fig. 8, the average stable undercooling increases from 80 to 180 K when the melt undergoes the L–LST. The same effect is also observed in $\text{Co}_{76}\text{Sn}_{24}$ alloy [8] and the other two compositions of Co–B alloys [42]. The recent nucleation model proposed by TOURNIER [85–87], was applied to explaining the experimental results of Co–B alloys

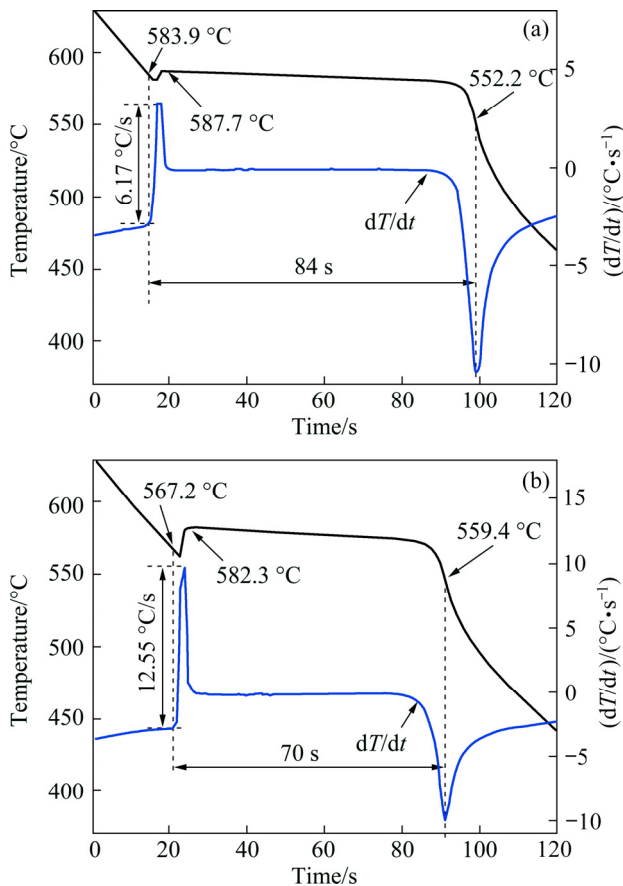


Fig. 7 Cooling curves for $\text{Bi}_2\text{Te}_{2.7}\text{Se}_{0.3}$ liquid alloy (The initial melt is prepared by heating to a temperature higher (a) or less (b) than L–LST temperature) [32]

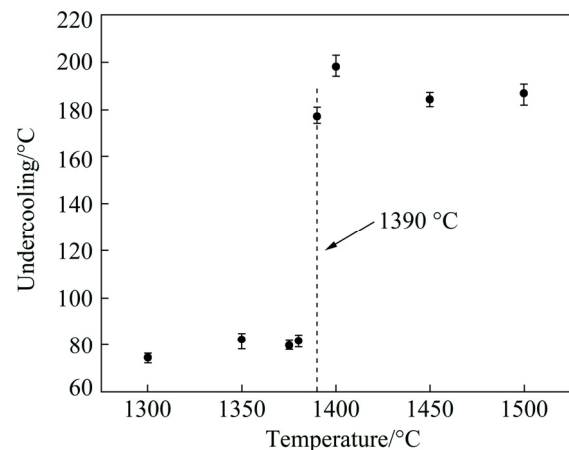


Fig. 8 Mean undercooling of $\text{Co}_{83}\text{B}_{17}$ alloy processed at different overheating temperatures [7]

and it was found to be satisfactory [42]. TOURNIER insisted that tiny crystals can be survival up to a critical temperature T_{m2} which is above the melting point T_m due to the energy saving ε_V per volume unit produced by the equalization of Feimi energies of crystals and their melt. These crystals act as the intrinsic nuclei in the undercooled melts and their presence reduces the critical energy barrier. As a result, the undercooling needed is much smaller when the overheating temperature is below T_{m2} . A brief introduction of this model to calculate T_{m2} is expressed as follows.

The interface electrostatic energy ε_V is taken to be part of the contributions to the volume free energy change ΔG_V . Thus, the total Gibbs free energy change for the formation of a nuclei with a radius R is given as

$$\Delta G_{ls}(T) = (\Delta G_V - \varepsilon_V)4\pi R^3 / 3 + 4\pi R^2 \sigma_{ls} \quad (3)$$

where $\Delta G_V = \Delta H_m \theta / V_m$, $\sigma_{ls} (V_m / N_A)^{-1/3} = \alpha_{ls} \Delta H_m / V_m$ and $\theta = T / T_m - 1$.

The critical radius R^* for nucleation can be obtained if the partial derivation of ΔG_{ls} with respect to R is set to be zero, i.e.,

$$\frac{\partial \Delta G_{ls}(T)}{\partial R} = 0 \quad (4)$$

Consequently, the R^* is derived as

$$R^* = -2 \frac{\sigma_{ls}}{\Delta G_V - \varepsilon_V} \quad (5)$$

A non-dimensional parameter ε_{ls} is introduced to evaluate the contribution by ε_V , i.e., $\varepsilon_V = \varepsilon_{ls} \Delta H / V_m$. Therefore, the R^* can be expressed as

$$R^* = -2 \frac{\alpha_{ls}}{\theta - \varepsilon_{ls}} \left(\frac{V_m}{N_A} \right)^{1/3} \quad (6)$$

As can be seen from Eq. (6), the R^* is positive when $\theta < \varepsilon_{ls}$ and negative when $\theta > \varepsilon_{ls}$, indicating that the tiny crystals can be survival up to a so-called second melting temperature T_{m2} , which is $T_{m2} = (1 + \varepsilon_{ls})T_m$. The relation between ε_{ls} and θ is given as $\varepsilon_{ls} = 0.217(1 - 2.5\theta^2)$

Then, so-called second melting temperature T_{m2} can be calculated. The calculated results are consistent with the experimental results, indicating that the anomaly of undercooling is caused by the un-melted tiny crystals surviving up to the critical temperature T_{m2} where the L–LST takes place.

These survived tiny crystals in the liquid act as

a template, catalyzing the nucleation. To reduce the nucleation barrier, the new phase with the structure close to the local structure in the liquid tends to nucleate first, even it is metastable. KELTON et al [6] demonstrated an enhanced icosahedral SRO with decreasing temperature in Ti–Zr–Ni liquids that form icosahedral quasicrystals (*i*-phase), decreasing the barrier for the nucleation of the metastable *i*-phase, even over the formation of stable polytetrahedral crystal phases. The first recalescence is due to the formation of a metastable *i*-phase that transforms after 2–3 s to the C14 Laves phase (the second recalescence), as shown in Fig. 9.

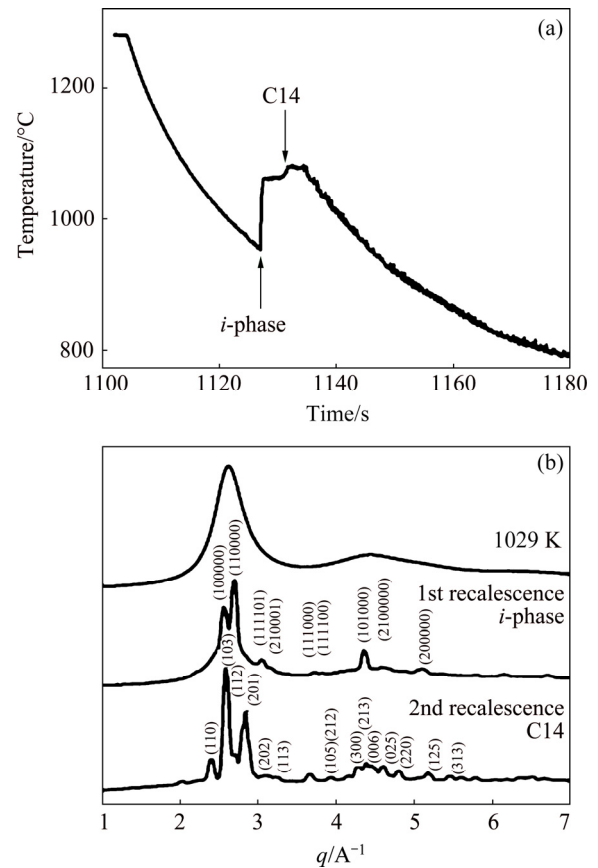


Fig. 9 Cooling curve for electrostatically-levitated 2.5 mm droplet of $Ti_{39.5}Zr_{39.5}Ni_{21}$ with temperature as function of time, showing two recalescence events (a) and X-ray diffraction pattern as function of momentum transfer q for undercooled liquid Ti–Zr–Ni alloy at 1029 K and during first and second recalescence (b) [6]

4.2 Crystallization products and microstructure

The L–LST has significant impacts on the solidification structures and there are growing experimental supports for the feasibility of changing the liquid state, based on the L–LST, to modify the solidification microstructures. Figure 10

shows the solidification microstructures of Bi–10 wt.%Sb alloy [88]. The primary phase of sample solidified from the melt without L–LST (Fig. 10(a)) is obviously coarse and the morphology is irregular, while the primary phase of sample solidifying from the melt experiencing L–LST is fine and uniform (Fig. 10(b)). As we mentioned above, the atomic bonds of crystals are only partly broken on melting and the SROs similar to the corresponding solid crystal remain in liquids within a certain temperature range. These SROs are beneficial to becoming the nuclei to promote nucleation and growth of crystal during cooling, owing to the convenient structure and energy fluctuation. Besides, it is worth mentioning that the liquid is inhomogeneous since the SROs are different in shape and size. Therefore, the microstructure morphology is irregular and coarse when the alloy is melted below the L–LST temperature. As the temperature increasing, atoms obtain more and more kinetic energy. Up to the L–LST temperature, the energy is large enough to overcome the energy barrier and the SROs disintegrate and break up,

resulting in a relatively homogeneous and disordered liquid. This kind of liquid is difficult to meet the need of nucleation and thus a greater undercooling degree is needed. According to the classical nucleation theory, the density of critical nucleus and nucleation rate will be higher with a greater undercooling. Furthermore, the growth rate is slower due to the lower atom diffusion rate resulting from the great undercooling. Therefore, the morphology is fine and uniform when the alloy is melted above the L–LST temperature.

The grain refining effect caused by the L–LST is evidenced in several alloys. The same effect can also be applicable for eutectic alloys. Figure 11 shows the microstructures of the Sn₅₇Bi₄₃ eutectic alloy solidified from different liquid states [89]. The microstructure of the sample experiencing the L–LST has a degree of refinement and the lamellar spacing of eutectic structures decreases significantly. Similar refinement phenomenon is observed in the Sn₇₅Bi₂₅ hypoeutectic alloy [90]. The lamellar spacing of eutectic structures decrease from 7.6 to 2.1 μm after the L–LST, as shown in Fig. 12.

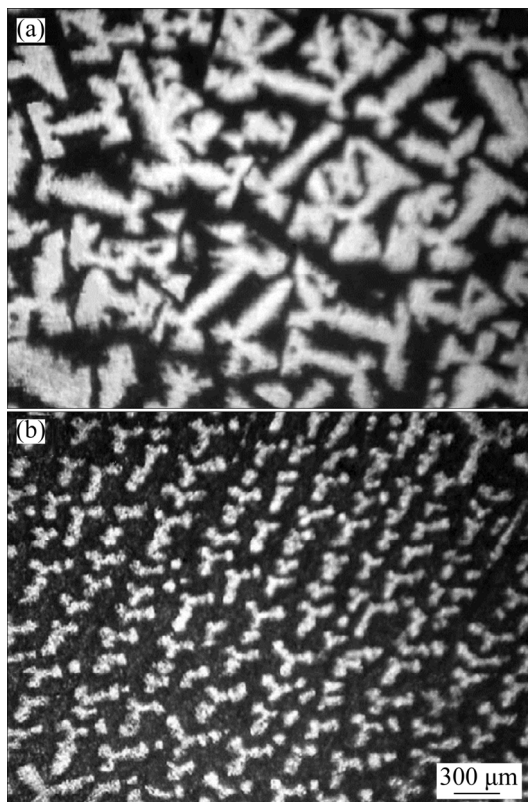


Fig. 10 Solidification microstructures of Bi–10wt.%Sb alloy observed by optical microscopy (The initial melts are prepared by heating to a temperature less (a) or higher (b) than L–LST temperature) [88]

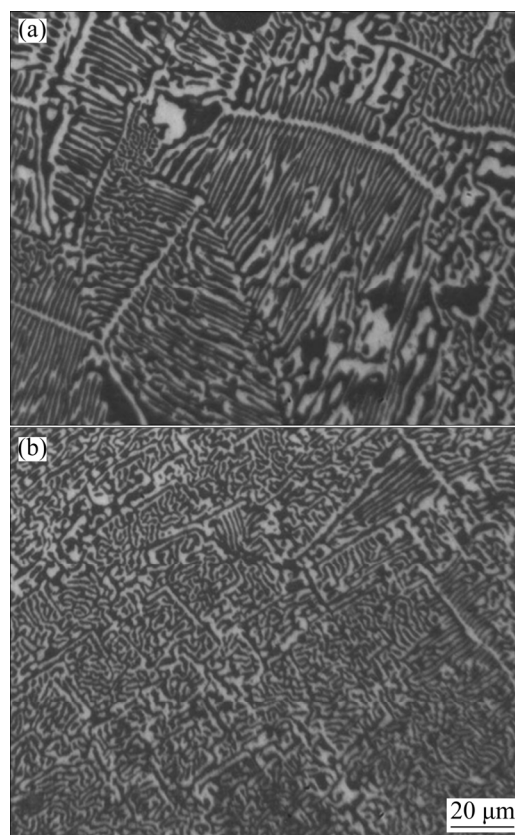


Fig. 11 Solidification microstructures of Sn₅₇Bi₄₃ eutectic alloy (The initial melts are prepared by heating to a temperature less (a) or higher (b) than L–LST temperature) [89]

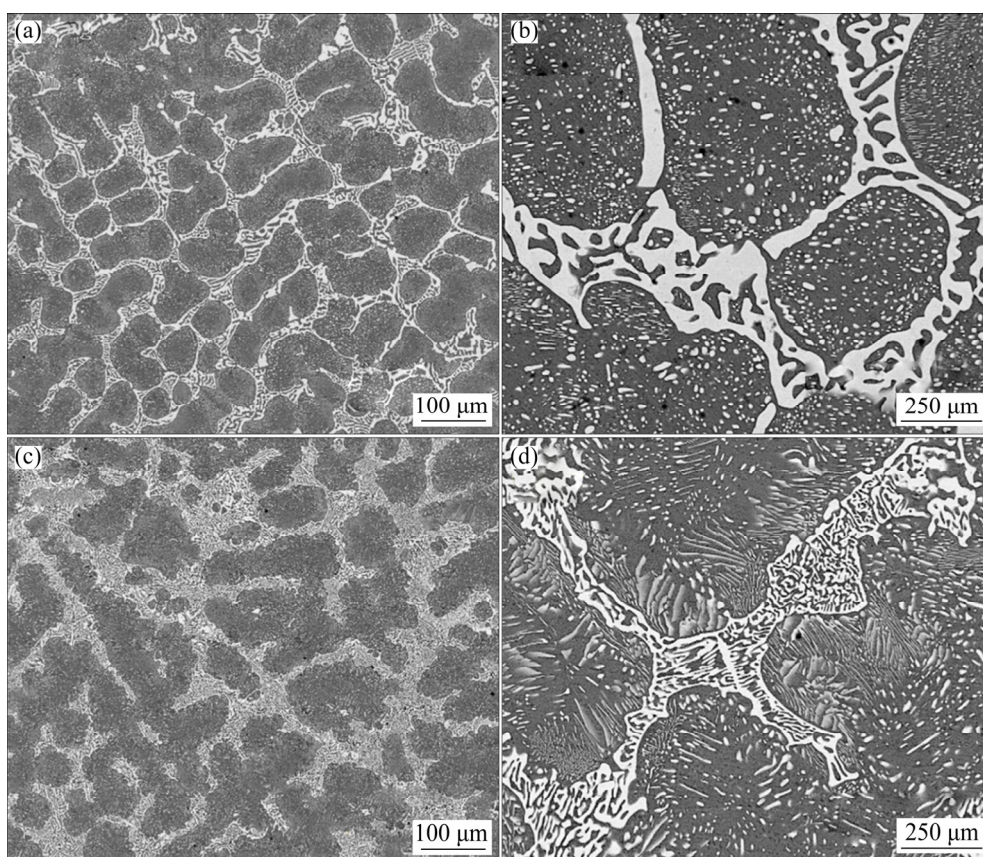


Fig. 12 Solidification microstructures of Sn₇₅Bi₂₅ hypoeutectic alloy (The initial melt is prepared by heating to a temperature less (a, b) or higher (c, d) than L–LST temperature) [90]

There are many local favored atomic pairs corresponding to different SROs, since the atoms of constituent element do not distribute uniformly in metallic liquid. The SRO composed of local favored atomic pair acts as pre-existent nuclei, which can directly grow and form corresponding nanocrystalline phases. The crystallization production is related to the configuration of SRO and the number of different SROs. As mentioned above, the configuration of SRO and the number of different SROs evolve with increasing the temperature, especially at the L–LST temperature. Therefore, the crystallization products can also be altered by the L–LST. The DSC curves of three Ti₄₀Zr₂₅Ni₈Cu₉Be₁₈ metallic glass rods prepared at different liquid temperatures are shown in Fig. 13(a) [91]. The melting temperature of Ti₄₀Zr₂₅Ni₈Cu₉Be₁₈ metallic glass is around 1020 K. The endothermic signal peak (indicated by the arrow) is only observed on the curve of Rod 1, which may be due to the difference in crystallization products forming during the first crystallization process. For Rod 1, *i*-phase forms during first crystallization and this

metastable *i*-phase transforms to the stable Laves phase at high temperature through the endothermic reaction. However, for Rod 2 and Rod 3, a stable phase rather than metastable *i*-phase forms directly from amorphous matrix. The XRD patterns of Rod 1 and Rod 2 after isothermal annealing confirm the hypothesis, as shown in Figs. 13(b, c). For Rod 1, some new peaks appear after first crystallization, which is typical diffraction pattern of *i*-phase. However, there is no typical diffraction pattern of *i*-phase in XRD pattern after first crystallization for Rod 2. The difference in crystallization products indicates that Rod 1 and Rod 2 possess different initial microstructures, i.e., different liquid states. It can be inferred that there is a temperature induced L–LST between 1123 K (Rod 1) and 1573 K (Rod 2), which has a significant influence on the crystallization products.

4.3 Glass forming ability

In recent years, there has been growth in the supportive evidence of L–LST in metallic glass-forming liquids from both experiments and

computer simulations [47,79,87,92–95]. It is found that the structure evolution during L–LST is beneficial to the glass forming ability. By using the concept of the superheated fragility of melts, ZHAO et al [79] introduced a transition strength parameter F , the ratio of the fragility of the HTZ (M_H) to that of the LTZ (M_L), which can be used to describe the characteristic of L–LST. Based on the viscosity data in Fig. 6(d), the M_H , M_L and the corresponding F values can be fitted. After systematically studying the dependence of F on the glass forming ability of ten Cu–Zr alloys, it is found that there is a close relationship between F and the glass-forming ability: the bigger the value of F , the stronger the glass-forming ability.

Combined with the simulation results, it is believed that the glass-forming ability is closely related to the abrupt increase of i -phase. A general scenario shown in Fig. 14 is proposed. When the L–LST with a large value of F happens, more initial local structures break partly down, reform into Z12 and lead to a more stable disordered system, decreasing the ability of crystallization, but increasing the glass-forming ability. When the L–LST with a small value of F happens, most of local structures own higher energy and lower density relative to Z12, and the average size of the clusters becomes much larger, leading to an increase of relatively unstable clusters in the LTZ. These unstable clusters are difficult to freeze into amorphous structures due to

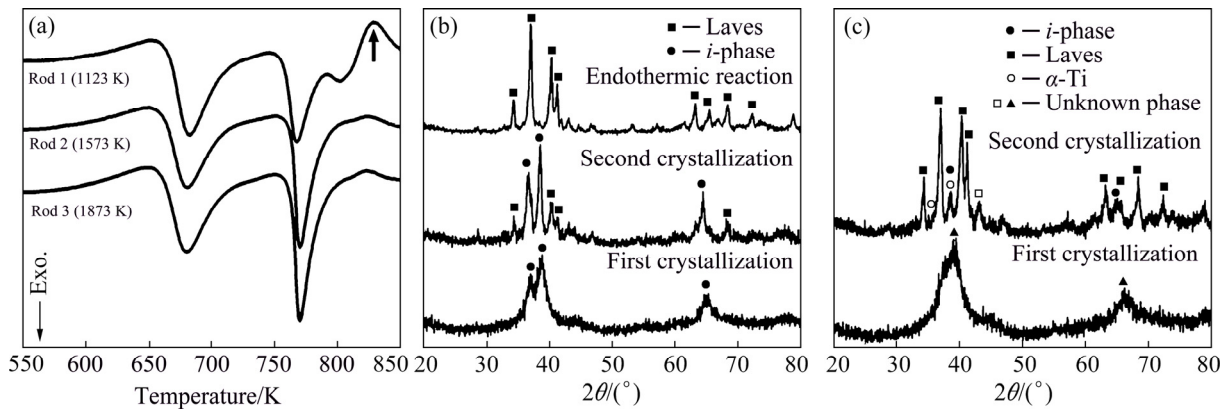


Fig. 13 DSC curves of three $Ti_{40}Zr_{25}Ni_8Cu_9Be_{18}$ metallic glass rods prepared at different liquid temperatures (a), and XRD patterns of Rod 1 (b) and Rod 2 (c) after isothermal annealing [91]

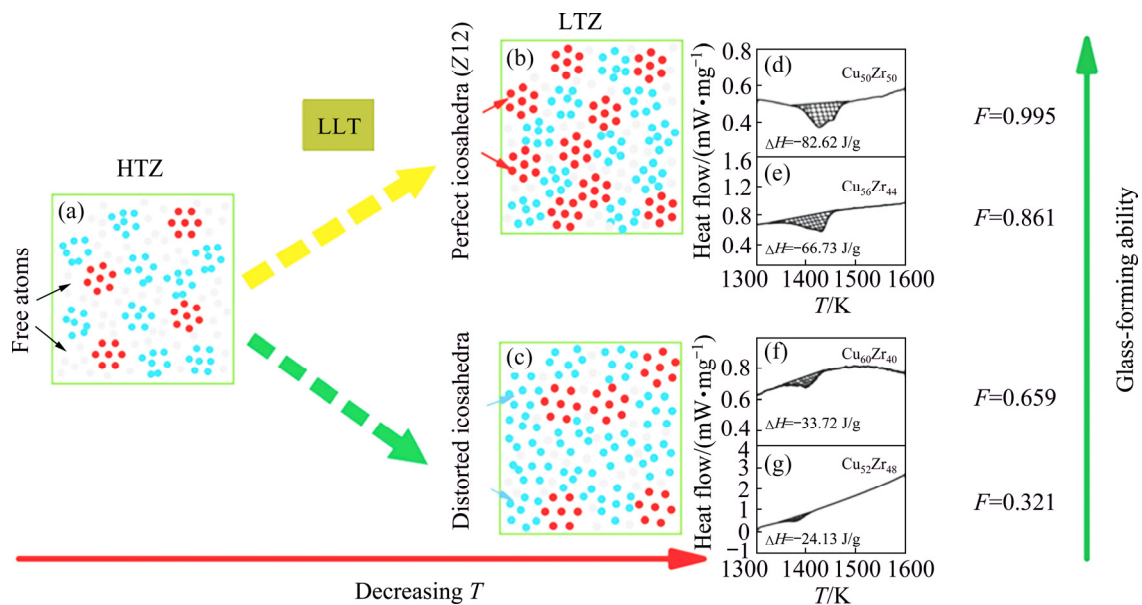


Fig. 14 Schematic structural evolution scenario accompanying L–LST in Cu–Zr melts and energy levels of liquids before (a) and after (b, c) L–LST, and DSC curves upon cooling for four Cu–Zr compositions (d–g) (The corresponding F values fitted from the viscosity data are shown in the right of each curve) [79]

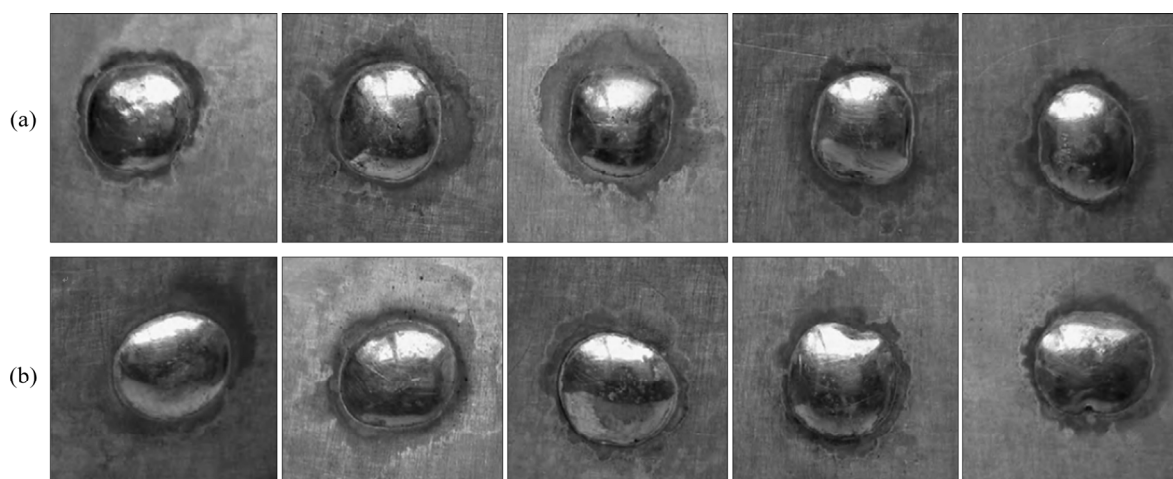


Fig. 15 Spread ability testing of Sn–Cu solders (The initial melts are prepared by heating to a temperature less (a) or higher (b) than L–LST temperature) [96]

a relatively weak resistance against structural degradation during further cooling. The DSC measurements for different compositions with different values of F confirm the scenario. For $\text{Cu}_{60}\text{Zr}_{40}$ and $\text{Cu}_{52}\text{Zr}_{48}$ alloys, the value of F is relatively smaller than that for $\text{Cu}_{50}\text{Zr}_{50}$ and $\text{Cu}_{56}\text{Zr}_{44}$, and the heat released during the L–LST is less, which can be observed from the shadow regions in Figs. 14(d–g). The more the heat is released accompanying the L–LST, the larger the glass-forming ability is.

4.4 Properties

Since the L–LST has large influence on the nucleation, crystallization products and microstructure as we mentioned above, it is reasonable to conjecture that these alterations might lead to an enhancement of the properties of commercial-scale ingots, thus benefitting to applications.

(1) Wettability

LI et al [96] studied the effect of L–LST on the wettability of Sn–0.7Cu solder, and they found that the wettability was improved when the sample solidified from the melt experiencing the L–LST. The overall spreading area in Fig. 15(b) is larger than that of Fig. 15(a), which is thought to be due to the melt experiencing L–LST is more disordered and homogeneous, and the atoms are more active. The same effect is also observed in Sn–3.8Ag–0.7Cu– x Ce ($x=0, 0.2, 0.5$ and 1.0 , wt.%) melts [97].

(2) Corrosion resistance

With increasing melt temperature, the corrosion potential (ϕ_{corr}) of $\text{Al}_{97}\text{La}_3$ alloy ribbon

increases and the corrosion current density (J_{corr}) decreases, as shown in Fig. 16 [98]. With the increase of temperature, the melt structure becomes more uniform and random, and the atomic cluster becomes small, which is retained in rapidly solidified alloys. Therefore, the corrosion resistance is improved with the more uniform structure prepared by melt heat treatment.

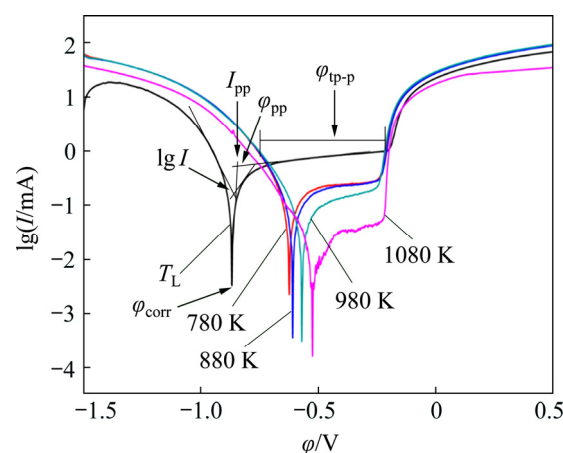


Fig. 16 Potentiodynamic polarization curves of $\text{Al}_{97}\text{La}_3$ alloy prepared at different liquid temperatures (The T_L of $\text{Al}_{97}\text{La}_3$ alloy is around 680 K) [98]

(3) Mechanical properties

Figure 17 presents compressive engineering strain–stress curve of $\text{Ti}_{40}\text{Zr}_{25}\text{Ni}_8\text{Cu}_9\text{Be}_{18}$ metallic glass rods prepared at different liquid temperatures [91]. As described earlier in Fig. 13, Rod 1 was prepared without the process of L–LST and Rod 2 experienced the L–LST. As shown in Fig. 17, the plasticity of Rod 1 is larger than that of

Rod 2, although they exhibit same elastic limit about 2.3% and yield strength near 1900 MPa. Other mechanical properties are also found to be affected by the L–LST, such as the hardness [32], and the tensile properties [99].

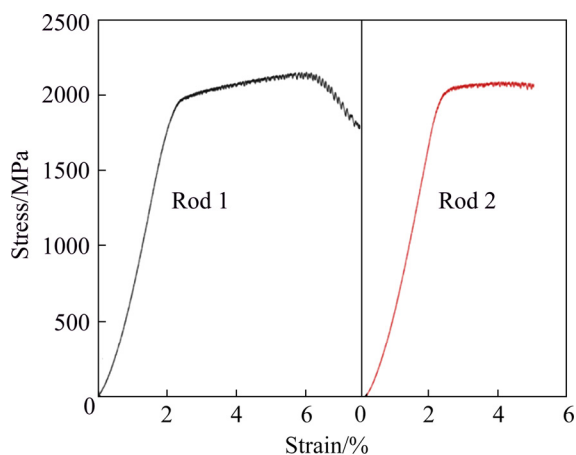


Fig. 17 Compressive engineering strain–stress curves of $\text{Ti}_{40}\text{Zr}_{25}\text{Ni}_8\text{Cu}_9\text{Be}_{18}$ metallic glass rods [91]

5 Conclusions and outlook

As opposed to the conventional view of liquids that liquid structures and properties change gradually with temperature and pressure, with different means, temperature or pressure induced discontinuous liquid structure transitions were observed to occur in many metals and alloys. The classification of L–LST can be based on the inducing condition, the reversibility of the transition process and the thermodynamic property of the transition. Experimental methods on L–LST can be classified into direct methods and indirect methods.

Controlling the liquid states, based on the L–LSTs, has been confirmed to be effective in regulating the subsequent solidification processes, microstructures and properties. This provides a promising approach to manipulate the materials with desired microstructure and outstanding properties, even when only a simple solidification process is performed.

In the future, the mechanism of L–LST needs to be further understood. More adequate models of liquid structure, especially for those systems with the L–LST, are essential for the simulation and experimental research. Moreover, the relationship between the L–LST and the abnormal change of physical parameters requires to be clarified.

Acknowledgments

The author, Yi-xuan HE, gratefully acknowledges financial support from the China Scholarship Council (CSC). We acknowledge the support of the LNCMI-CNRS, member of the European Magnetic Field Laboratory (EMFL).

References

- [1] ZHAI Wei, CHANG Jian, GENG De-lu, WEI Bing-bo. Progress and prospect of solidification research for metallic materials [J]. *The Chinese Journal of Nonferrous Metals*, 2019, 29(9): 1953–2008. (in Chinese)
- [2] ZU Fang-qiu, CHEN Jie, LI Xian-fen, MAO Li-na, LIU Yong-chi. A new viewpoint to the mechanism for the effects of melt overheating on solidification of Pb–Bi alloys [J]. *Journal of Materials Research*, 2009, 24(7): 2378–2384.
- [3] GENG Hao-ran, ZHANG Guo-ling, WANG Zhi-ming, DENG Yan-bo, QIN Hai-ou. Density–temperature properties of Ga–Sb alloy melt [J]. *Applied Physics A*, 2010, 98(1): 227–232.
- [4] QIN Jing-yu, QIN Xu-bo, WANG Wei-min, BIAN Xiu-fang. Model on medium range order in liquid Al–Fe alloys [J]. *Transactions of Nonferrous Metals Society of China*, 2004, 14(6): 1068–1073.
- [5] STOLPE M, JONAS I, WEI Shuai, EVENSON Z, HEMBREE W, YANG Fan, MEYER A, BUSCH R. Structural changes during a liquid–liquid transition in the deeply undercooled $\text{Zr}_{58.5}\text{Cu}_{15.6}\text{Ni}_{12.8}\text{Al}_{10.3}\text{Nb}_{2.8}$ bulk metallic glass forming melt [J]. *Physical Review B*, 2016, 93(1): 014201.
- [6] KELTON K F, LEE G W, GANGOPADHYAY A K, HYERS R W, RATHZ T J, ROGERS J R, ROBINSON M B, ROBINSON D S. First X-ray scattering studies on electrostatically levitated metallic liquids: Demonstrated influence of local icosahedral order on the nucleation barrier [J]. *Physical Review Letters*, 2003, 90(19): 195504.
- [7] WANG Jun, HE Yi-xuan, LI Jin-shan, HU Rui, KOU Hong-chao, BEAUGNON E. Overheating dependent undercooling in a hypoeutectic Co–B alloy [J]. *Materials Chemistry and Physics*, 2015, 149–150: 17–20.
- [8] QIU Xiao-xing, LI Jin-shan, WANG Jun, GUO Tong, KOU Hong-chao, BEAUGNON E. Effect of liquid–liquid structure transition on the nucleation in undercooled Co–Sn eutectic alloy [J]. *Materials Chemistry and Physics*, 2016, 170: 261–265.
- [9] LI Meng-wan, HUANG Yong-jiang, XUE Peng, JIANG Song-shan, RU Wei-nan, YANG Zhi-qin, YIN H, DAISENBERGER D, SHEN Hong-xian, SUN Jian-fei. Temperature-induced atomic structural evolution in a liquid Ga-based alloy [J]. *Vacuum*, 2019, 170: 108966.
- [10] REN Nan-nan, SHANG Bao-shuang, GUAN Peng-fei, HU Li-na. General structural and dynamic characteristics beneficial to glass-forming ability of Fe-based glass-forming liquids [J]. *Journal of Non-Crystalline Solids*, 2018, 481: 116–122.

- [11] KATAYAMA Y, MIZUTANI T, UTSUMI W, SHIMOMURA O, YAMAKATA M, FUNAKOSHI K I. A first-order liquid-liquid phase transition in phosphorus [J]. *Nature*, 2000, 403(6766): 170–173.
- [12] ZHANG Shi-liang, WANG Li-min, ZHANG Xin-yu, QI Li, ZHANG Su-hong, MA Ming-zhen, LIU Ri-ping. Polymorphism in glassy silicon: Inherited from liquid-liquid phase transition in supercooled liquid [J]. *Scientific Reports*, 2015, 5: 8590.
- [13] MURATA K I, TANAKA H. Microscopic identification of the order parameter governing liquid-liquid transition in a molecular liquid [J]. *Proceedings of the National Academy of Sciences*, 2015, 112(19): 5956–5961.
- [14] MOSSES J, SYME C D, WYNNE K. Order parameter of the liquid-liquid transition in a molecular liquid [J]. *The Journal of Physical Chemistry Letters*, 2015, 6(1): 38–43.
- [15] McMILLAN P F, WILSON M, DAISENBERGER D, MACHON D. A density-driven phase transition between semiconducting and metallic polyamorphs of silicon [J]. *Nature Materials*, 2005, 4: 680–684.
- [16] ZHAO Gang, YU Y J, TAN X M. Nature of the first-order liquid-liquid phase transition in supercooled silicon [J]. *The Journal of Chemical Physics*, 2015, 143(5): 054508.
- [17] WU C J, GLOSLI J N, GALLI G, REE F H. Liquid-liquid phase transition in elemental carbon: A first-principles investigation [J]. *Physical Review Letters*, 2002, 89(13): 135701.
- [18] KHAN S, WANG X D, CAO Q P, ZHANG D X, JIANG J Z. Structural evolution in liquid calcium under pressure [J]. *Journal of Non-Crystalline Solids*, 2017, 472: 25–30.
- [19] INUI M, KAJIHARA Y, HOSOKAWA S, MATSUDA K, TSUCHIYA Y, TSUTSUI S, BARON A Q R. Dynamical sound speed and structural inhomogeneity in liquid Te studied by inelastic X-ray scattering [J]. *Journal of Non-Crystalline Solids: X*, 2019, 1: 100006.
- [20] WANG Jun, LI Jin-shan, HU Rui, KOU Hong-chao, BEAUGNON E. Evidence for the structure transition in a liquid Co–Sn alloy by in-situ magnetization measurement [J]. *Materials Letters*, 2015, 145: 261–263.
- [21] KOGA K, TANAKA H, ZENG X C. First-order transition in confined water between high-density liquid and low-density amorphous phases [J]. *Nature*, 2000, 408: 564–567.
- [22] WU Wei-kang, ZHANG Lei-ning, LIU Si-da, REN Hong-ru, ZHOU Xu-yan, LI Hui. Liquid-liquid phase transition in nanoconfined silicon carbide [J]. *Journal of the American Chemical Society*, 2016, 138(8): 2815–2822.
- [23] LO Y F, WANG X C, WU Z D, ZHOU W Z, KUI H W. Direct imaging of a first-order liquid-liquid phase transition in undercooled molten PdNiP alloys and its thermodynamic implications [J]. *Journal of Non-Crystalline Solids*, 2017, 472: 75–85.
- [24] LI Xin-xin, WANG Jin, QIN Jing-yu, DONG Bang-shao, PAN Shao-peng. The reassessment of the structural transition regions along the liquidus of Fe–Si alloys and a possible liquid-liquid structural transition in FeSi₂ alloy [J]. *Physics Letters A*, 2018, 382(37): 2655–2661.
- [25] CHENG Su-juan, BIAN Xiu-fang, ZHANG Jing-xiang, QIN Xu-bo, WANG Zhong-hua. Correlation of viscosity and structural changes of indium melt [J]. *Materials Letters*, 2003, 57(26–27): 4191–4195.
- [26] WANG Li, BIAN Xiu-fang, LIU Jian-tong. Discontinuous structural phase transition of liquid metal and alloys (1) [J]. *Physics Letters A*, 2004, 326(5–6): 429–435.
- [27] WANG Li, LIU Jian-tong. Discontinuous structural phase transition of liquid metal and alloys (2) [J]. *Physics Letters A*, 2004, 328(2–3): 241–245.
- [28] WU Yu-qin, BIAN Xiu-fang, MENG Qing-ge, ZHAO Yan, MAO Tan, ZHANG Yan-ning. A critical transition state in liquid metals [J]. *Materials Letters*, 2007, 61(11–12): 2434–2438.
- [29] TANAKA H. General view of a liquid-liquid phase transition [J]. *Physical Review E*, 2000, 62(5): 6968–6976.
- [30] XU Wei, SANDOR M, YU Yao, KE Hai-bo, ZHANG Hua-ping, LI Mao-zhi, WANG Wei-hua, LIU Lin, WU Yue. Evidence of liquid-liquid transition in glass-forming La₅₀Al₃₅Ni₁₅ melt above liquidus temperature [J]. *Nature Communications*, 2015, 6: 7696.
- [31] LI Xiao-yun, XU Fang-qiu, WU Wei, ZHANG Xian-feng, FENG Da-shun. Liquid-liquid structure transition in Sn–3.5Ag–3.5Bi melts [J]. *Phase Transitions*, 2012, 85(12): 1091–1097.
- [32] YU Yuan, WU Zhao, COJOCARU-MIRÉDIN O, ZHU Bin, WANG Xiao-yu, GAO Na, HUANG Zhong-yue, ZU Fang-qiu. Dependence of solidification for Bi₂Te_{3–x}Se_x alloys on their liquid states [J]. *Scientific Reports*, 2017, 7(1): 2463.
- [33] LAN S, BLODGETTL M, KELTON K, MA J L, FAN J, WANG X L. Structural crossover in a supercooled metallic liquid and the link to a liquid-to-liquid phase transition [J]. *Applied Physics Letters*, 2016, 108(21): 211907.
- [34] XIONG L H, WANG X D, YU Q, ZHANG H, ZHANG F, SUN Y, CAO Q P, XIE H L, XIAO T Q, ZHANG D X, WANG C Z, HO K, REN Y, JIANG J Z. Temperature-dependent structure evolution in liquid gallium [J]. *Acta Materialia*, 2017, 128: 304–312.
- [35] KIM T H, KELTON K F. Structural study of supercooled liquid transition metals [J]. *The Journal of Chemical Physics*, 2007, 126(5): 054513.
- [36] WANG W Y, HAN J J, FANG H Z, WANG J, LIANG Y F, SHANG S L, WANG Y, LIU X J, KECSKES L, MATHAUDHU S, HUI X, LIU Z K. Anomalous structural dynamics in liquid Al₈₀Cu₂₀: An ab initio molecular dynamics study [J]. *Acta Materialia*, 2015, 97: 75–85.
- [37] ZHAO G, MU H F, TAN X M, WANG M S, WANG D H, YANG C L. First-order liquid-liquid phase transition in AsS melt caused by change of intermediate-range order [J]. *Journal of Non-Crystalline Solids*, 2014, 404: 135–139.
- [38] IWASHITA T, NICHOLSON D M, EGAMI T. Elementary excitations and crossover phenomenon in liquids [J]. *Physical Review Letters*, 2013, 110(20): 205504.
- [39] ZU Fang-qiu. Temperature-induced liquid-liquid transition in metallic melts: A brief review on the new physical phenomenon [J]. *Metals*, 2015, 5(1): 395–417.
- [40] KOBAYASHI M, TANAKA H. The reversibility and first-order nature of liquid-liquid transition in a molecular liquid [J]. *Nature Communications*, 2016, 7: 13438.
- [41] JIA Peng, ZHANG Jin-yang, TENG Xin-ying, ZHAO De-gang, WANG Yi, HU Song, XIANG Jun, ZHANG Shu, HU Xun. Liquid phase transition of Sn₅₀Bi₅₀ hypereutectic

- alloy and its thermodynamic and kinetic aspects [J]. *Journal of Molecular Liquids*, 2018, 251: 185–189.
- [42] HE Yi-xuan, LI Jin-shan, WANG Jun, KOU Hong-chao, BEAUGNON E. Liquid–liquid structure transition and nucleation in undercooled Co–B eutectic alloys [J]. *Applied Physics A*, 2017, 123(6): 391.
- [43] DEMMEL F, FRAILE A, SZUBRIN D, PILGRIM W C, MORTEL C. Experimental evidence for a dynamical crossover in liquid aluminium [J]. *Journal of Physics: Condensed Matter*, 2015, 27(45): 455102.
- [44] le COQ D, BYTCHKOV A, HONKIMÄKI V, BEUNEU B, BYCHKOV E. Neutron and X-ray diffraction studies of TeCl_4 and TeBr_4 liquids [J]. *Journal of Non-Crystalline Solids*, 2008, 354(2): 259–262.
- [45] HOLLAND-MORITZ D, SCHENK T, CONVERT P, HANSEN T, HERLACH D M. Electromagnetic levitation apparatus for diffraction investigations on the short-range order of undercooled metallic melts [J]. *Measurement Science and Technology*, 2005, 16(2): 372–380.
- [46] KIMURA H, WATANABE M, IZUMI K, HIBIYA T, HOLLAND-MORITZ D, SCHENK T, BAUCHSPIEß K R, SCHNEIDER S, EGRY I, FUNAKOSHI K, HANFLAND M. X-ray diffraction study of undercooled molten silicon [J]. *Applied Physics Letters*, 2001, 78: 604–606.
- [47] GE Jia-cheng, HE Hai-yan, ZHOU Jing, LU Chen-yu, DONG Wei-xia, LIU Si-nan, LAN Si, WU Zhen-duo, WANG An-ding, WANG Liang, YU Cun, SHEN Bao-long, WANG Xun-li. In-situ scattering study of a liquid–liquid phase transition in Fe–B–Nb–Y supercooled liquids and its correlation with glass-forming ability [J]. *Journal of Alloys and Compounds*, 2019, 787: 831–839.
- [48] GREAVES G N, WILDING M C, FEARN S, KARGL F, HENNET L, BRAS W, MAJÉRUS O, MARTIN C M. Liquid–liquid transitions, crystallization and long range fluctuations in supercooled yttrium oxide–aluminium oxide melts [J]. *Journal of Non-Crystalline Solids*, 2009, 355(10): 715–721.
- [49] LAHIRI D, SHARMA S M, VERMA A K, VISHWANADH B, DEY G K, SCHUMACHER G, SCHERB T, RIESEMEIER H, REINHOLZ U, RADTKE M, BANERJEE S. Investigation of short-range structural order in $\text{Zr}_{69.5}\text{Cu}_{12}\text{Ni}_{11}\text{Al}_{7.5}$ and $\text{Zr}_{41.5}\text{Ti}_{41.5}\text{Ni}_{17}$ glasses, using X-ray absorption spectroscopy and ab initio molecular dynamics simulations [J]. *Journal of Synchrotron Radiation*, 2014, 21: 1296–1304.
- [50] LUO W K, MA E. EXAFS measurements and reverse Monte Carlo modeling of atomic structure in amorphous $\text{Ni}_{80}\text{P}_{20}$ alloys [J]. *Journal of Non-Crystalline Solids*, 2008, 354(10): 945–955.
- [51] ZOU P F, WANG H P, YANG S J, HU L, WEI B B. Anomalous temperature dependence of liquid state density for $\text{Ni}_{50}\text{Ti}_{50}$ alloy investigated under electrostatic levitation state [J]. *Chemical Physics Letters*, 2017, 681: 101–104.
- [52] BREAUX G A, NEAL C M, CAO B, JARROLD M F. Melting, premelting, and structural transitions in size-selected aluminum clusters with around 55 atoms [J]. *Physical Review Letters*, 2005, 94: 173401.
- [53] ZU F Q, ZHU Z G, GUO L J, ZHANG B, SHUI J P, LIU C S. Liquid–liquid phase transition in Pb–Sn melts [J]. *Physical Review B*, 2001, 64(18): 180203.
- [54] HE Yi-xuan, LI Jin-shan, WANG Jun, YILDIZ E, PAIRIS S, BEAUGNON E. Temperature-induced structure transition in a liquid Co–B eutectic alloy [J]. *Materials Letters*, 2019, 234: 351–353.
- [55] LIU Rong-xue, JIA Peng, LI Ming-yang, GENG Hao-ran, LENG Jin-feng. Structure transition of $\text{Sn}_{57}\text{Bi}_{43}$ melt and its thermodynamic and kinetic characteristics [J]. *Materials Letters*, 2015, 145: 108–110.
- [56] ZHOU Chao, HU Li-na, SUN Qi-jing, QIN Jing-yu, BIAN Xiu-fang, YUE Yuan-zheng. Indication of liquid-liquid phase transition in CuZr-based melts [J]. *Applied Physics Letters*, 2013, 103(17): 171904.
- [57] LIU B B, HU L, WANG Z Y, YE F. Viscosity, relaxation and fragility of the $\text{Ca}_{65}\text{Mg}_{15}\text{Zn}_{20}$ bulk metallic glass [J]. *Intermetallics*, 2019, 109: 8–15.
- [58] BELTYUKOV A, LADYANOV V, STERKHOVA I. Effect of small nickel additions on viscosity of liquid aluminum [J]. *Journal of Molecular Liquids*, 2019, 296: 111764.
- [59] LI J J Z, RHIM W K, KIM C P, SAMWER K, JOHNSON W L. Evidence for a liquid–liquid phase transition in metallic fluids observed by electrostatic levitation [J]. *Acta Materialia*, 2011, 59(5): 2166–2171.
- [60] WANG Jun, HE Yi-xuan, LI Jin-shan, HU Rui, KOU Hong-chao, BEAUGNON E. Experimental platform for solidification and in-situ magnetization measurement of undercooled melt under strong magnetic field [J]. *The Review of Scientific Instruments*, 2015, 86(2): 025102.
- [61] HE Yi-xuan, LI Jin-shan, LI Li-yuan, WANG Jun, YILDIZ E, BEAUGNON E. Composition dependent characteristic transition temperatures of Co–B melts [J]. *Journal of Non-Crystalline Solids*, 2019, 522: 119583.
- [62] OKAMOTO H. B–Co (boron–cobalt) [J]. *Journal of Phase Equilibria*, 2003, 24(4): 376.
- [63] SMALLENBURG F, FILION L, SCIORTINO F. Erasing no-man’s land by thermodynamically stabilizing the liquid–liquid transition in tetrahedral particles [J]. *Nature Physics*, 2014, 10(9): 653–657.
- [64] WANG W L, WU Y H, LI L H, ZHAI W, ZHANG X M, WEI B. Liquid–liquid phase separation of freely falling undercooled ternary Fe–Cu–Sn alloy [J]. *Scientific Reports*, 2015, 5: 16335.
- [65] PALMER J C, MARTELLI F, LIU Y, CAR R, PANAGIOTOPOULOS A Z, DEBENEDETTI P G. Metastable liquid-liquid transition in a molecular model of water [J]. *Nature*, 2014, 510(7505): 385–388.
- [66] HE Ye-zeng, LI Hui, JIANG Yan-yan, LI Xiong-ying, BIAN Xiu-fang. Liquid–liquid phase transition and structure inheritance in carbon films [J]. *Scientific Reports*, 2014, 4: 3635.
- [67] YANG Sui, SU Xu-ping, WANG Jian-hua, YIN Fu-cheng, LI Zhi, CHEN Shang-da, LIU Can. Temperature-evolution of structure and diffusion properties of liquid transition metals [J]. *Journal of Non-Crystalline Solids*, 2010, 356(20): 1061–1069.
- [68] MO Yun-fei, TIAN Ze-an, LANG Lin, LIU Rang-su, ZHOU Li-li, HOU Zhao-yang, PENG Ping, ZHANG Tian-yi. The short-range order in liquid and A15 crystal of zirconium [J]. *Journal of Non-Crystalline Solids*, 2019, 513: 111–119.

- [69] QIAO C, GUO Y R, WANG J J, SHEN H, WANG S Y, ZHENG Y X, ZHANG R J, CHEN L Y, WANG C Z, HO K M. Pressure induced short-range structural changes in supercooled liquid $\text{Ge}_2\text{Sb}_2\text{Te}_5$ [J]. *Journal of Non-Crystalline Solids*, 2019, 503–504: 382–388.
- [70] NORITAKE F, KAWAMURA K. Structural transformations in sodium silicate liquids under pressure: A molecular dynamics study [J]. *Journal of Non-Crystalline Solids*, 2016, 447: 141–149.
- [71] WANG Zhi-chao, DUAN Yun-rui, LI Tao, ZHANG Li-shu, DAI Xin-yue, ZHANG Xing-fan, LIU Yao, JIANG Yan-yan, LI Hui. Liquid–liquid phase transition in nanoconfined Si-rich SiO_2 liquids [J]. *Computational Materials Science*, 2018, 154: 426–434.
- [72] HOU Zhao-yang, LIU Rang-su, XU Chun-long, SHUAI Xue-min, SHU Yu. Molecular dynamics simulation of relationship between local structure and dynamics during glass transition of Mg_7Zn_3 alloy [J]. *Transactions of Nonferrous Metals Society of China*, 2014, 24(4): 1086–1093.
- [73] LIU Rang-su, LIANG Yong-chao, LIU Hai-rong, ZHENG Nai-chao, MO Yun-fei, HOU Zhao-yang, ZHOU Li-li, PENG Ping. Simulation study on non-linear effects of initial melt temperatures on microstructures during solidification process of liquid Mg_7Zn_3 alloy [J]. *Transactions of Nonferrous Metals Society of China*, 2013, 23(4): 1052–1060.
- [74] ZHOU Li-li, LIU Rang-su, TIAN Ze-an. Simulation of formation and evolution of nano-clusters during rapid solidification of liquid $\text{Ca}_{70}\text{Mg}_{30}$ alloy [J]. *Transactions of Nonferrous Metals Society of China*, 2013, 23(8): 2354–2360.
- [75] ZHANG Qi, WANG Jin-cheng, TANG Sai, WANG Yu-jian, LI Jun-jie, ZHOU Wen-quan, WANG Zhi-jun. Molecular dynamics investigation of the local structure in iron melts and its role in crystal nucleation during rapid solidification [J]. *Physical Chemistry Chemical Physics*, 2019, 21(8): 4122–4135.
- [76] QIN Jing-yu, PAN Shao-peng, QI Yuan-hua, GU Ting-kun. The structure and thermodynamic properties of liquid Al–Si alloys by ab initio molecular dynamics simulation [J]. *Journal of Non-Crystalline Solids*, 2016, 433: 31–37.
- [77] TASCI E S, SLUITER M H F, PASTUREL A, VILLARS P. Liquid structure as a guide for phase stability in the solid state: Discovery of a stable compound in the Au–Si alloy system [J]. *Acta Materialia*, 2010, 58(2): 449–456.
- [78] MASSOBRIO C, van ROON F H M, PASQUARELLO A, de LEEUW S W. Breakdown of intermediate-range order in liquid GeSe_2 at high temperatures [J]. *Journal of Physics: Condensed Matter*, 2000, 12(46): L697–L704.
- [79] ZHAO Xi, WANG Chun-zhen, ZHENG Hai-jiao, TIAN Ze-an, HU Li-na. The role of liquid–liquid transition in glass formation of CuZr alloys [J]. *Physical Chemistry Chemical Physics*, 2017, 19(24): 15962–15972.
- [80] ZU Fang-qiu, ZHOU Bing, LI Xian-fen, YI Xun, CHEN Yi-ping, SUN Qi-qiang. Effect of liquid–liquid structure transition on solidification of Sn–Bi alloys [J]. *Transactions of Nonferrous Metals Society of China*, 2007, 17(5): 893–897.
- [81] TIAN Xue-lei, LI Cheng-dong, CHEN Xi-chen, LIU Feng, ILINSKY A. Structures of bulk amorphous $\text{Zr}_{41}\text{Ti}_{14}\text{Ni}_{10}\text{Cu}_{12.5}\text{Be}_{22.5}$ alloy in amorphous, crystalline, supercooled liquid and liquid states [J]. *Transactions of Nonferrous Metals Society of China*, 2002, 12(1): 34–37.
- [82] RUSSO J, TANAKA H. Crystal nucleation as the ordering of multiple order parameters [J]. *The Journal of Chemical Physics*, 2016, 145(21): 211801.
- [83] KELTON K F, GREER A L, HERLACH D M, HOLLAND-MORITZ D. The influence of order on the nucleation barrier [J]. *MRS Bulletin*, 2004, 29(12): 940–944.
- [84] LI Xiao-yun, ZU Fang-qiu, GAO Wen-long, CUI Xiao, WANG Li-fang, DING Guo-hua. Effects of the melt state on the microstructure of a Sn–3.5%Ag solder at different cooling rates [J]. *Applied Surface Science*, 2012, 258(15): 5677–5682.
- [85] TOURNIER R F. Presence of intrinsic growth nuclei in overheated and undercooled liquid elements [J]. *Physica B: Condensed Matter*, 2007, 392(1–2): 79–91.
- [86] TOURNIER R F. Crystallization of supercooled liquid elements induced by superclusters containing magic atom numbers [J]. *Metals*, 2014, 4(3): 359–387.
- [87] TOURNIER R F. Predicting glass-to-glass and liquid-to-liquid phase transitions in supercooled water using classical nucleation theory [J]. *Chemical Physics*, 2018, 500: 45–53.
- [88] LI Xian-feng, ZU Fang-qiu, YU Jin, ZHOU Bing. Effect of liquid–liquid transition on solidification of Bi–10 wt% Sb alloy [J]. *Phase Transitions*, 2008, 81(1): 43–50.
- [89] LI Ming-yang, ZHANG Yong-xing, WU Chen, GENG Hao-ran. Effect of liquid–liquid structure transition on solidification of $\text{Sn}_{57}\text{Bi}_{43}$ alloy [J]. *Applied Physics A*, 2016, 122: 171.
- [90] JIA Peng, LI Xue-li, ZHANG Jin-yang, ZHANG Kai, TENG Xin-ying, HU Xun, YANG Cheng, ZHAO De-gang. Liquid–liquid structure transition and its effect on the solidification behaviors and microstructure of $\text{Sn}_{75}\text{Bi}_{25}$ alloy [J]. *Journal of Molecular Liquids*, 2018, 263: 218–227.
- [91] ZHOU Xun, KOU Hong-chao, WANG Jun, LI Jin-shan, ZHOU Lian. Crystallization and compressive behaviors of $\text{Ti}_{40}\text{Zr}_{25}\text{Ni}_8\text{Cu}_9\text{Be}_{18}$ BMG cast from different liquid states [J]. *Intermetallics*, 2012, 28: 45–50.
- [92] LUCAS P. Fragile-to-strong transitions in glass forming liquids [J]. *Journal of Non-Crystalline Solids: X*, 2019, 4: 100034.
- [93] REN Nan-nan, HU Li-na, WANG Li-jin, GUAN Peng-fei. Revealing a hidden dynamic signature of the non-Arrhenius crossover in metallic glass-forming liquids [J]. *Scripta Materialia*, 2020, 181: 43–47.
- [94] WANG Jian-guo, CHANG Chun-tao, SONG Kai-kai, WANG Li, PAN Ye. Short-range ordering in metallic supercooled liquids and glasses [J]. *Journal of Alloys and Compounds*, 2019, 770: 386–394.
- [95] ZHENG Hai-jiao, LV Yu-miao, SUN Qi-jing, HU Li-na, YANG Xiu-nan, YUE Yuan-zheng. Thermodynamic evidence for cluster ordering in $\text{Cu}_{46}\text{Zr}_{42}\text{Al}_7\text{Y}_5$ ribbons during glass transition [J]. *Science Bulletin*, 2016, 61(9): 706–713.
- [96] LI Xian-feng, ZHANG Fei, ZU Fang-qiu, LV Xue, ZHAO Zhen-xing, YANG Dong-dong. Effect of liquid–liquid

- structure transition on solidification and wettability of Sn-0.7Cu solder [J]. Journal of Alloys and Compounds, 2010, 505(2): 472–475.
- [97] LIU Xiao-guang, JIANG Xiao-ming, CAO Li-chao, ZHAI Wen-gang, LI Xian-feng, WEI Zhou. Microstructure and properties of Sn-3.8Ag-0.7Cu-xCe lead-free solders with liquid-liquid structure transition and Ce addition [J]. Materials Research Express, 2019, 6(11): 1165b8.
- [98] LI Ming-yang, JIA Peng, LIU Rong-xue, GENG Hao-ran, DU Song-zhao, WANG Ming-xu, LUO Hong, LU Shu-jing. The effect of melt overheating on the melt structure transition and solidified structures of Al-La alloy [J]. The Journal of the Minerals, Metals & Materials Society, 2015, 67(5): 948–954.
- [99] CHEN Zhi-hao, ZHENG Wei, ZU Fang-qiu, ZHU Xie-bing, SUN Yu-feng. Influence of liquid structure change on microstructure and properties of SnZnBi solder alloy [J]. Advanced Materials Research, 2012, 463–464: 489–493.

金属熔体中的液-液结构转变现象及其对凝固的影响

贺一轩^{1,2}, 李金山¹, 王军¹, Eric BEAUGNON²

1. 西北工业大学 凝固国家重点实验室, 西安 710072;

2. Université Grenoble Alpes, INSA Toulouse, Université Toulouse Paul Sabatier,
EMFL, CNRS, LNCMI, 38000 Grenoble, France

摘要: 液态合金结构和性质的研究一直是凝聚态物理和金属材料科学领域的重要研究方向之一。液态合金并非理想的均质液体, 在温度和压力等作用下会发生不连续转变。液-液结构转变广泛存在于金属和合金中, 并且对最终凝固组织和性能有着很大的影响。系统阐释金属熔体中液-液结构转变现象, 总结液-液结构转变对最终凝固组织和宏观性能的影响等方面的主要研究进展。结果表明, 利用熔体液-液结构转变可以有效调控金属及合金的组织, 改善其宏观性能。

关键词: 液-液结构转变; 金属及合金; 热历史; 凝固

(Edited by Bing YANG)